

Title:	Compressive Behaviour of Geopolymer Concrete-Filled Steel Columns at Ambient and Elevated Temperatures
Authors:	Zhong Tao, Centre for Infrastructure Engineering, University of New South Wales Yi-Fang Cao, Centre for Infrastructure Engineering, University of New South Wales Zhu Pan, Centre for Infrastructure Engineering, University of New South Wales Md Kamrul Hassan, Centre for Infrastructure Engineering, University of New South Wales
Subjects:	Building Materials/Products Fire & Safety Structural Engineering
Keywords:	Composite Fire Safety Strength-Testing Structure
Publication Date:	2018
Original Publication:	International Journal of High-Rise Buildings Volume 7 Number 4
Paper Type:	1. Book chapter/Part chapter 2. Journal paper 3. Conference proceeding 4. Unpublished conference paper 5. Magazine article 6. Unpublished

Compressive Behaviour of Geopolymer Concrete-Filled Steel Columns at Ambient and Elevated Temperatures

Zhong Tao[†], Yi-Fang Cao, Zhu Pan, and Md Kamrul Hassan

Centre for Infrastructure Engineering, Western Sydney University, Penrith, NSW 2751, Australia

Abstract

Geopolymer concrete (GPC), which is recognised as an environmentally friendly alternative to ordinary Portland cement (OPC) concrete, has been reported to possess high fire resistance. However, very limited research has been conducted to investigate the behaviour of geopolymer concrete-filled steel tubular (GCFST) columns at either ambient or elevated temperatures. This paper presents the compressive test results of a total of 15 circular concrete-filled steel tubular (CFST) stub columns, including 5 specimens tested at room temperature, 5 specimens tested at elevated temperatures and the remaining 5 specimens tested for residual strength after exposure to elevated temperatures. The main variables in the test program include: (a) concrete type; (b) concrete strength; and (c) curing condition of geopolymer concrete. The test results demonstrate that GCFST columns have similar ambient temperature behaviour compared with the conventional CFST counterparts. However, GCFST columns exhibit better fire resistance than the conventional CFST columns. Meanwhile, it is found that the GCFST column made with heat cured GPC has lower strength loss than other columns after exposure to elevated temperatures. The research results highlight the possibility of using geopolymer concrete to improve the fire resistance of CFST columns.

Keywords: Concrete-filled steel tubes, Stub columns, Geopolymer concrete, Fire resistance, Residual strength

1. Introduction

Concrete-filled steel tubular (CFST) columns have been widely used as main structural elements in multi-storey and high-rise buildings to carry loads. Because of the composite action between the steel and core concrete, this type of composite construction has been reported to have many constructional and structural benefits, such as easy construction for the omission of formwork, high strength, large stiffness and high ductility (Han et al., 2014).

Accidental fire remains a high risk for building structures, which may lead to civilian casualties and high cost for repairing structural damage. In the worst scenario, uncontrolled fire can cause local or global collapse of a building (Wang et al., 2012). Despite their excellent performance at room temperature, unprotected CFST columns are usually not able to maintain structural integrity for sufficient time under fire conditions (Tao et al., 2016). Therefore, external insulating coating and/or internal reinforcing steel are often required to improve the fire resistance of CFST columns (Wang et al., 2012). But these two methods tremendously increase the cost of CFST columns and raise the difficulty of construction.

Although ordinary Portland cement (OPC) concrete is classified as a fire-resistant construction material, severe

spalling may occur for this material in fire (Kodur and Phan, 2007). Meanwhile, fire exposure also leads to significant deterioration of its strength and stiffness. More recently, geopolymer concrete (GPC) has been developed as an environmentally friendly alternative to OPC concrete. Geopolymer is an aluminosilicate binder which is synthesised through a reaction of a solid material of geological origin (e.g., metakaolin) or industry by-products (e.g., fly ash) with alkaline solutions (Habert et al., 2011). Previous studies (Shaikh and Vimonsatit, 2015; Pan and Sanjavan, 2012; Vickers et al., 2016) have demonstrated that geopolymer can be successfully used as a binder to make GPC, which generally has better fire performance than OPC concrete. This is owing to the fact that geopolymer has a three-dimensional network structure of interconnected aluminate and silicate tetrahedra, which is very stable at elevated temperatures (Pan et al., 2018). In contrast, dehydration occurs in the OPC system at high temperature, which is irreversible after heating beyond 500°C (Vickers et al., 2016; Kodur and Phan, 2007). Therefore, geopolymer concrete has the potential to be used in CFST columns to improve their fire performance, which may eliminate the use of external insulating coating or internal reinforcing bars for the CFST columns.

Some recent studies have been conducted to investigate the structural behaviour of GPC in load-bearing members, such as beams (Sumajouw and Rangan, 2006), columns (Sumajouw and Rangan, 2006; Sumajouw et al., 2007) and slabs (Ataei et al., 2016). However, the majority of these

[†]Corresponding author: Zhong Tao
Tel: +61-2-4736-0064
E-mail: z.tao@westernsydney.edu.au

studies were conducted on reinforced GPC members (Mo et al., 2016), whilst composite structures fabricated from GPC have received little attention among researchers.

Shi et al. (2015) carried out an experimental investigation on short geopolymeric recycled concrete-filled steel columns with a square cross-section. The test results were compared with those of CFST columns made with cement-based recycled aggregate concrete. In their research, the two types of concrete developed similar compressive strengths at the time of testing. However, it was reported that the load-carrying capacities of the geopolymer CFST columns were 23–26% higher than those of the cement-based CFST columns when no recycled aggregate was added to the concrete. On the other hand, both geopolymer and cement-based CFST columns had comparable load-carrying capacities when 50% or 100% natural coarse aggregate was replaced by recycled aggregate. Another research finding reported by Shi et al. (2015) is that geopolymer CFST columns had smaller peak strains corresponding to the peak loads compared with the cement-based CFST counterparts.

Ozbakkaloglu and Xie (2016) reported experimental results of 36 concrete-filled square fibre-reinforced polymer tubes tested under axial compression. These specimens were prepared using either OPC or fly ash-based geopolymer concrete. In general, the concrete type had little influence on the compressive strength of the composite columns. However, the columns fabricated from GPC exhibited a lower ultimate axial strain than the reference samples manufactured with OPC. The latter also demonstrated a marked plateau in the transition regions of their stress-strain curves due to a large shrinkage of the OPC. In contrast, the GPC samples did not have an obvious plateau in the curve since the shrinkage of the GPC was much smaller.

Espinos et al. (2015) conducted a numerical analysis to investigate the fire performance of concrete-filled double-tube columns. For a typical OPC-filled double-tube column, the predicted fire resistance time is 87 min. When GPC presents at the ring between the inner and the outer steel tubes, the predicted fire resistance time increases to 139 min. Espinos et al. (2015) attributed the increase in fire resistance to the delay in the temperature rise of the inner tube because of the outer geopolymer concrete. In their simulation, a relatively low thermal conductivity of 0.43 W/m K was adopted for GPC. In contrast, the values of thermal conductivity for OPC concrete encased in a steel tube are 2.29, 1.26, and 0.74 W/m K at 20, 500, and 1000°C, respectively, according to a model proposed in (Tao and Ghannam, 2013). The difference in thermal conductivity between the two materials partly explains the difference in predicted fire resistance time.

The above literature review indicates that no test results of circular GCFST columns have been reported. Meanwhile, no fire or post-fire tests have been carried out on GCFST columns. To address the research gaps, a series of ambient temperature and fire tests were conducted on circular GCFST columns. Reference specimens made with OPC concrete were also tested to compare with the GCFST specimens. A finite element (FE) model previously developed for conventional CFST columns will be tentatively applied to predict the ambient temperature behaviour of GCFST columns.

2. Experimental Investigation

2.1. Raw Materials of Concrete

Raw materials used in the manufacture of GPC include fly ash, calcium aluminate cement (CAC), alkali activator composed of NaOH and Na₂SiO₃ solution, fine aggregate

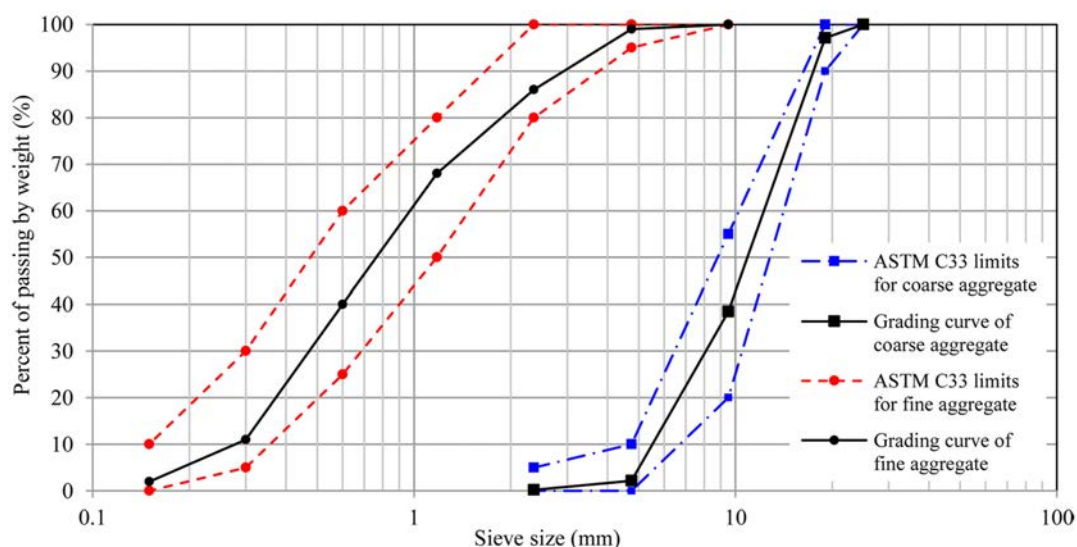


Figure 1. Sieve analysis of coarse and fine aggregates.

Table 1. Chemical composition of fly ash and CAC

Material	Al ₂ O ₃	SiO ₂	Fe ₂ O ₃	CaO	MgO	SO ₃	K ₂ O	Na ₂ O
Fly ash	30.5	48.3	12.1	2.8	1.2	0.3	0.2	0.4
CAC	75.3	0.1	0.3	20.9	2.1	0.2	0.1	1.0

and coarse aggregate. The coarse aggregate is crushed limestone, whereas the fine aggregate is natural river sand mined from the bed of a local river in Sydney. Both types of aggregates are well-graded, and the gradation meets the requirements of ASTM C33, as shown in Fig. 1. The fly ash used for making geopolymer came from a power station in Queensland, Australia and the chemical composition is shown in Table 1. The fly ash contains mainly quartz and Al₂O₃ (aluminium oxide). It can be characterised as ASTM Type F (low calcium) fly ash, as the sum of the oxides (Al₂O₃+SiO₂+Fe₂O₃) is more than 70% and the CaO content is less than 10%. CAC is an important type of non-Portland cement, and has rapid hardening characteristics and wide applications in refractory materials. In this study, CAC was used to replace part of fly ash to improve the mechanical properties of GPC and eliminate the need of heat curing. This has been proved in our preliminary research (Cao et al., 2016). The market brand of the CAC used in the test program is Secar 71 produced in Tianjin, China; the chemical composition is presented in Table 1. The CAC consists of less than 1% SiO₂ (quartz), but its alumina content (75.3%) is much higher than that (30.5%) in the fly ash. With the addition of CAC, the Al/Si ratio of the geopolymer will be increased, which may promote the geopolymerisation process (Cao et al., 2016).

The geopolymer samples were prepared using alkaline solution consisting of alkali (Na) hydroxide and commercially available sodium silicate solution. The sodium silicate, namely water glass, was grade D solution with a SiO₂/Na₂O modulus equal to 2 (where Na₂O = 14.7%, and SiO₂ = 29.4% by mass). The sodium hydroxide solution was prepared by dissolving NaOH pellets into tap water. The activator was prepared beforehand and stored for 24 h before use to form a homogenous solution.

General-purpose Portland cement produced in Australia was used to make the reference OPC concrete. High range water reducing admixture (MasterGlenium SKY 8100) in an aqueous solution was used for improving the workability of the OPC concrete. MasterGlenium SKY 8100 is a polycarboxylic ether polymer superplasticiser and complies with AS 1478.1 type high range water reducer.

2.2. Specimen Preparation

2.2.1. Proportions of Concrete Mixes

To accelerate strength development, low calcium fly ash-based geopolymer concrete normally requires heat curing as the dissolution rate of fly ash is slow at ambient temperature (Pan et al., 2018). Heat curing can be employed to make precast concrete members. For example, thirty-three heat-cured precast geopolymer concrete slabs were used

in the construction of the office building of the University of Queensland's Global Change Institute. The heat curing procedure, however, significantly limits the on-site application of geopolymer concrete. To develop ambient-cured geopolymer concrete, some additives, such as OPC or ground granulated blast furnace slag (GGBFS), need to be added to provide extra Ca²⁺ or Al³⁺ to promote reactions at ambient temperature (Pan et al., 2018). For example, the Toowoomba Wellcamp Airport in Australia was built using more than 40,000 m³ geopolymer concrete, where the heat curing regime was eliminated by adding GGBFS in the geopolymer concrete. In this research, CAC was selected as the additive to facilitate the ambient temperature curing. As both the heat cured and ambient cured geopolymer concretes have their applications in engineering, these two curing methods were used in the current research for preparing the samples.

Four geopolymer concrete mixes and one reference OPC concrete mix were prepared, and the corresponding mix proportions are shown in Table 2. It should be noted that CAC was only used in mixes GPC-1, GPC-2 and GPC-3 to allow the development of strength of GPC at ambient temperature. For comparison purposes, a conventional GPC mix GPC-4 was also prepared without the addition of CAC. This mix was heat cured at 80°C for 24 h to assist the strength development. The strength of ambient cured GPC was adjusted by changing the alkalinity of the activator and the amount of CAC in the mix. The alkalinity of the activator was controlled by the amount of sodium hydroxide in the GPC mix, as shown in Table 2. Based on our preliminary research results reported in (Cao et al., 2016), GPC-1 was designed to have the lowest amounts of sodium hydroxide and CAC, whereas GPC-3 has the highest amounts of these ingredients. GPC-2 was designed to have medium amounts of sodium hydroxide and CAC. As a result, GPC-1 achieved the lowest compressive strength among the three mixes, whilst GPC-3 had the highest compressive strength. It should be noted that extra water of 30.9 kg/m³ was added to GPC-2 to improve its workability. This ensures that its strength and workability are comparable to those of the reference OPC concrete based on trial mixes. Meanwhile, the heat cured GPC-4 has similar mix proportions to GPC-2, except that no CAC was added to GPC-4.

2.2.2. Design of CFST Stub Columns

A total of 15 circular CFST stub columns were prepared, including 5 specimens tested at room temperature, 5 specimens tested at elevated temperatures and the remaining 5 specimens tested for residual strength after exposure

Table 2. Proportions of concrete mixes (kg/m³)

Specimen label	NaOH pellet (kg)	Water (kg)	Sodium silicate (kg)	Fly ash (kg)	Cement (kg)	CAC (kg)	Coarse aggregate (kg)	Fine aggregate (kg)	Extra water (kg)	Water reducer (L)
OPC	-	186.6	-	-	466.4	-	1131.3	614.2	-	1.6
GPC-1	19.8	43.3	157.6	465.6	-	24.0	1095.1	594.5	-	-
GPC-2	21.1	30.9	130.3	468.1	-	52.0	1080.3	586.5	30.9	-
GPC-3	25.6	37.6	157.6	441.4	-	49.0	1094.6	594.3	-	-
GPC-4 (Heat curing)	21.1	30.9	130.3	520.1	-	-	1080.3	586.5	30.9	-

Table 3. Summary of CFST stub column specimens

Test type	Label	D (mm)	t_s (mm)	f'_c (MPa)	Age (days)	N_{uc} (or $N_{u,r}$) (kN)	N_p (kN)	t_R (min)	Concrete type
Ambient strength test (Series 1)	CFT-OPC	150.0	3.01	59.2	31	1681.0	-	-	OPC
	CFT-GPC1	150.4	3.01	37.4	26	1207.5	-	-	GPC-1
	CFT-GPC2	149.6	3.01	58.6	29	1479.7	-	-	GPC-2
	CFT-GPC3	150.3	3.01	64.4	32	1649.9	-	-	GPC-3
	CFT-GPC4	150.2	3.01	31.8	30	1196.2	-	-	GPC-4
Residual strength test (Series 2)	RES-OPC	150.6	3.01	59.2	31 ^a	788.0	-	-	OPC
	RES-GPC1	149.6	3.01	37.4	26 ^a	528.0	-	-	GPC-1
	RES-GPC2	150.3	3.01	58.6	29 ^a	555.6	-	-	GPC-2
	RES-GPC3	150.8	3.01	64.4	32 ^a	553.0	-	-	GPC-3
	RES-GPC4	149.3	3.01	31.8	30 ^a	643.6	-	-	GPC-4
Elevated temperature test (Series 3)	HOT-OPC	150.6	3.01	59.2	31	-	841	36.7	OPC
	HOT-GPC1	150.2	3.01	37.4	26	-	604	60.1	GPC-1
	HOT-GPC2	150.8	3.01	58.6	29	-	740	44.3	GPC-2
	HOT-GPC3	149.5	3.01	64.4	32	-	825	37.5	GPC-3
	HOT-GPC4	149.9	3.01	31.8	30	-	598	85.4	GPC-4

^aConcrete age at the time of heat treatment.

to elevated temperatures. The specimen details are presented in Table 3. The main parameters investigated in the test program include: (a) concrete type (OPC concrete and geopolymers concrete); (b) concrete strength (31.8–64.4 MPa); and (c) curing condition of geopolymers concrete (ambient curing and heat curing). The first three letters in the specimen labels are used to differentiate the type of tests, where “CFT”, “RES” and “HOT” refer to test at ambient temperature (Series 1), test for measuring the residual strength after exposure to elevated temperatures (Series 2) and test in hot conditions (Series 3), respectively. The following letters and number (if any) in the label designate the concrete type. For example, CFT-GPC1 represents a specimen tested at ambient temperature and the concrete mix used is GPC-1.

All CFST specimens were designed to have a length (L) of 340 mm, which was intended to fit in the furnace equipped with an actuator. The nominal external diameter (D) of the steel tubes was 150 mm, and the nominal thickness (t_s) was 3 mm. Accordingly, the L/D ratio of the specimens was 2.26, which is slightly lower than the normal value of 3 used for stub columns. However, it has been reported in (Tao et al., 2013a) that when the L/D

ratio lies in the range of 2–5, its influence on the stub column behaviour is not obvious.

2.2.3. Fabrication of Steel Tubes

Mild steel sheets were used to cold form semi-circular tubes, and two such semi-circular tubes were then welded together to form a whole circular tube. Each circular tube was welded with two endplates with a diameter of 200 mm and a thickness of 12 mm. It should be noted that there was a hole with a diameter of 120 mm cut on the top endplate for pouring concrete. A Vernier calliper was used to measure the cross-sectional dimensions of the hollow tubes, and the measured dimensions are given in Table 3. In general, the measured dimensions are very close to the nominal values, indicating the high quality of fabrication. Three tensile coupons were cut from a steel tube to measure the material properties of steel.

2.2.4. Concrete Production and Placement

To make GPC, the binder (fly ash and CAC) and saturated surface dry aggregates were added together into a mixer and dry-mixed for 3 min. Afterwards, the specified extra water was added to the dry mix of GPC-2 or GPC-

4 to ensure adequate workability. The alkaline activator was then added, and the wet mixture was stirred for additional 4–6 min to form a homogenous state. The mixing procedure for the OPC concrete is similar to that of GPC, except that the water and superplasticiser were added in the mixer after the dry mix of aggregate and cement.

Concrete cylinders of 100 mm diameter and 200 mm height were cast for measuring the concrete compressive strength (f_c'). A vibrating table was employed to remove air bubbles from the concrete samples. The concrete cylinders were cast in two layers and each layer was vibrated for 15–30 s. The cast specimens were kept in moulds for 24 h at either ambient (for all mixes except GPC-4) or elevated (for GPC-4 only) temperatures. After demoulding, all cylindrical specimens were kept at ambient temperature and sealed in plastic bags until being tested. Prior to testing, the concrete cylindrical specimens were grinded using a CIVILAB core grinding machine to get smooth and flat ends.

The steel tubes were filled with different types of concrete presented in Table 2. During casting, a concrete vibrator was utilised to compact the concrete to expel the internal air bubbles. After casting, the CFST specimens along with the sealed concrete cylinders were stored together in the laboratory at ambient temperature. It is worth noting that the three specimens (CFT-GPC4, RES-GPC4 and HOT-GPC4) requiring a heat curing regime were first cured at 80°C for 24 h before being stored in the laboratory.

2.3. Test Setup

The compressive strength tests on concrete cylinders were conducted using a universal testing machine according to ASTM C39 (2001). The concrete age at the time of testing ranges from 26 to 39 days, as presented in Table 3. The corresponding CFST columns were also tested for ambient temperature strength (Series 1) or subjected to heat exposure (Series 2 and 3) on the same days. Therefore, the measured concrete strengths can represent the actual strengths of core concrete in the CFST columns.

For the CFST specimens tested at ambient temperature (Series 1 and 3), regardless of heat treatment, a total of four bidirectional strain gauges with a gauge length of 3 mm were attached to each specimen to measure the longitudinal and transverse strains of the steel tube at mid-height. Meanwhile, four linear variable displacement transducers (LVDT) were used to measure the column axial deformation. The compression test of the CFST columns was performed using a closed-loop servo controlled hydraulic MTS machine with a maximum capacity of 5000 kN, and the compression test setup is similar to that described in (Yu et al., 2016). A small preload of 10 kN was applied to the specimen with an aim to check the instrumentation and data logging system. Then the specimen was loaded continuously at a loading rate of 0.12 mm/min until reaching its peak load. In the post-peak range,

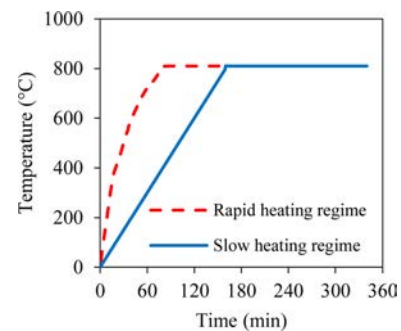


Figure 2. Heating regimes.

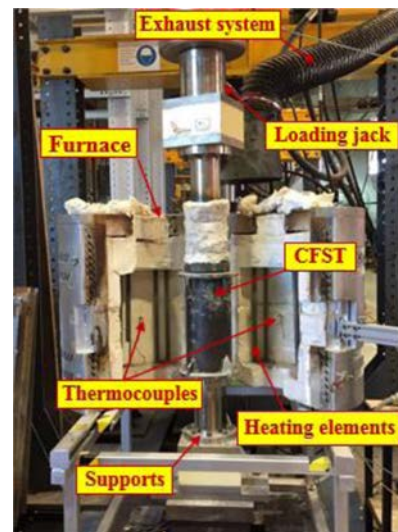


Figure 3. Split tube furnace.

the loading rate was increased to 0.6 mm/min until a sign of severe failure was observed in the specimen, such as severe bulging of the steel tube.

The heating of a specimen was conducted using an electrical split tube furnace, which has an external diameter of 630 mm and a height of 620 mm. The internal chamber of the furnace is 250 mm in diameter and 350 mm in height. A slow heating regime shown in Fig. 2 was used in the examination of CFST columns after exposure to elevated temperatures (Series 2). This heating regime has been commonly adopted to study the post-fire properties of cementitious materials (Li et al., 2017) and the behaviour of small-scale structural members after exposure to a target temperature (Han et al., 2002; Li et al., 2017). To study the residual strength, the CFST column was put inside the electrical furnace without loading, as shown in Fig. 3. Then the temperature of the furnace was increased to 800°C at a rate of 5°C/min, and this target temperature of 800°C was kept for 3 h to achieve an equilibrium state of temperature distribution in the specimen. After that, the specimen was naturally cooled to room temperature in the furnace. Finally, the specimen was tested at 7 d after

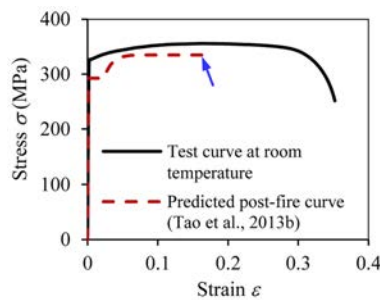


Figure 4. Stress-strain curves of steel.

cooling to investigate its post-fire behaviour.

The rapid heating regime shown in Fig. 2 was used to test the response of CFST columns at elevated temperatures with a constant load (Series 3). Ideally, the ISO 834 standard fire curve (ISO 834, 1999) should be followed using a gas furnace. However, gas furnaces are normally built to test large-scale specimens under ISO 834 fire exposure (Yang et al., 2008). Therefore, the current short CFST columns were tested in the electrical furnace at its highest heating rate (rapid heating regime). The load was applied using a MTS actuator, as shown in Fig. 3. The CFST column was first loaded to 50% of its ultimate load measured at ambient temperature, and the actual applied axial load (N_p) is shown in Table 3 for each relevant specimen. After the application of the axial load, the temperature was increased to 800°C within 80 min, and this temperature was maintained until the failure of the specimen. Due to the capacity of the furnace, the adopted heating regime has a much lower heating rate than the ISO 834 standard fire curve (ISO 834, 1999). However, this heating regime has been applied to all the five specimens tested at elevated temperatures. Therefore, the obtained test results can be used for comparing the fire performance of different CFST columns. Further experimental research, however, is still required to investigate the behaviour of large-scale GCFST columns under ISO 834 fire exposure.

2.4. Mechanical Properties of Steel and Concrete

The measured steel properties are: elastic modulus $E_s = 194,370$ MPa; yield stress $f_y = 326.0$ MPa; ultimate strength $f_u = 355.8$ MPa and corresponding ultimate strain $\epsilon_u = 0.172$; and the elongation = 0.371. A typical stress-strain (σ - ϵ) curve measured at room temperature is shown in Fig. 4. Meanwhile, the predicted σ - ϵ curve using a model presented in (Tao et al., 2013b) is also shown in this figure for the steel after exposure to 800°C. As can be seen, the steel shows obvious strength deterioration after the heat treatment. The predicted residual yield stress (f_{yT}) is 291.8 MPa, indicating a strength loss of 10.5%.

The cylinder compressive strengths (f'_c) of different concrete mixes are shown in Table 3. The values of f'_c for the ambient cured GPC mixes range from 37.4 to 64.4 MPa. The f'_c -value of the reference OPC concrete mix is



Figure 5. Failure modes of composite columns tested at room temperature.

59.2 MPa, which is close to that of GPC-2 (58.6 MPa). In contrast, the heat cured mix GPC-4 has the lowest f'_c of 31.8 MPa.

3. Test Results and Discussion

3.1. Performance of CFST Columns at Ambient Temperature

3.1.1. Failure Modes

The five specimens in Series 1 after testing at ambient temperature are shown in Fig. 5. All of them experienced a local outward folding failure. The local buckling occurred near the stiffeners either at the top or bottom. It seems the concrete type or strength has no influence on the failure mode.

3.1.2. Axial Load Versus Axial Strain Curves

The effects of concrete strength level, curing method of GPC and concrete type on the measured axial load versus axial strain (N - ϵ) curves are shown in Figs. 6-8, respectively. In these figures, the axial strain values were obtained from the measurements of strain gauges and LVDTs. The average values from the four axial strain gauges were implemented before the steel tube buckled. After that, the axial strain ϵ was calculated from average values of the four LVDTs divided by the overall length of the specimen. The steel yield strain ($\epsilon_y = 1680 \mu\epsilon$) measured from room temperature coupons is also indicated in these figures. Since the columns were designed to have a compact cross-section with a nominal D/t_s ratio of 50, the steel tubes had yielded before the columns reached their ultimate strengths. It can be inferred that the steel tubes have provided significant confinement to the concrete core (Tao et al., 2013a).

The comparison between the N - ϵ curves of GCFST columns with different strength levels is presented in Fig. 6. The concrete compressive strengths (f'_c) for CFT-GPC1, CFT-GPC2 and CFT-GPC3 are 37.4, 58.6 and 64.4 MPa, respectively. For GCFST columns with relatively high strength GPC (CFT-GPC2 and CFT-GPC3), the N - ϵ curve typically has an ascending branch, a descending branch and a stable branch. However, GCFST made with relatively low strength GPC (CFT-GPC1 with f'_c of 37.4 MPa) is

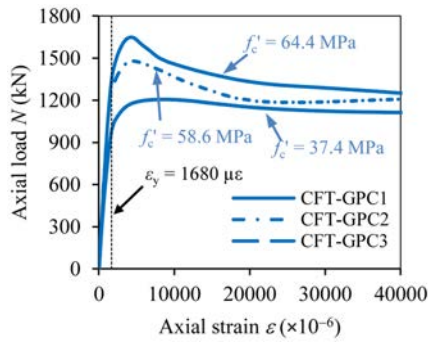


Figure 6. Comparison between N - ε curves of GCFST columns with different strength levels.

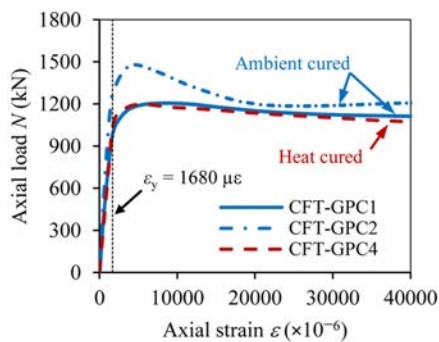


Figure 7. Comparison between N - ε curves of GCFST columns with different curing regimes.

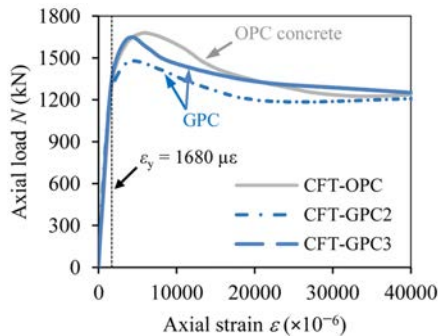


Figure 8. Comparison between N - ε curves of GCFST and conventional CFST columns.

seen to have no obvious descending branch before the curve reaches a stable residual response. It can be seen that the concrete strength has similar effects on the N - ε curves of both GCFST columns and conventional CFST columns.

The influence of different curing regimes on the N - ε performance of GCFST columns is illustrated in Fig. 7. The curing regimes for CFT-GPC1 and CFT-GPC2 are ambient curing, whereas CFT-GPC4 was cured at elevated temperature (80°C for 24 h). By comparison, CFT-GPC4 cured at elevated temperature exhibited a lower load-

bearing capacity than CFT-GPC2, although the mix designs of GPC in the two specimens are similar, except for the CAC addition in GPC-2. Compared with the compressive strength of GPC-4 (31.8 MPa), that of GPC-2 (58.6 MPa) is increased by 84% because of the use of CAC. Also shown in Fig. 7 is a comparison of N - ε performance between two columns with similar GPC compressive strengths (CFT-GPC1 and CFT-GPC4). The curves of the two GCFST columns almost superpose each other. The comparison indicates that the behaviour of ambient cured GCFST columns is similar to that of heat cured GCFST columns if the GPC strengths are relatively similar under two curing conditions.

Fig. 8 presents the influence of concrete type by comparing N - ε curves of two GCFST columns (CFT-GPC2 and CFT-GPC3) with that of the conventional CFST column (CFT-OPC). The compressive strength of the reference mix OPC (59.2 MPa) is between those of mix GPC-2 (58.6 MPa) and mix GPC-3 (64.4 MPa). However, the measured ultimate strength ($N_{uc} = 1681.0$ kN) for CFT-OPC is even slightly higher than that of CFT-GPC3 (1649.9 kN). This is likely due to testing error, which will be further analysed in subsection 3.1.7. If the discrepancy in the ultimate strength is ignored, the shapes of the N - ε curves for the two GPC specimens are similar to that of the conventional CFST column. However, the ultimate axial strains corresponding to the ultimate strengths for specimens CFT-GPC2 and CFT-GPC3 are 4530 and 4200 $\mu\epsilon$, respectively. These values are smaller than the corresponding strain (5860 $\mu\epsilon$) of CFT-OPC. This is consistent with the observations reported by Shi et al. (2015) and Ozbakkaloglu and Xie (2016). In general, the difference in ambient temperature behaviour between the GCFST and conventional CFST columns is not significant.

3.1.3. Ultimate Strength

The measured ultimate strengths (N_{uc}) of all columns are presented in Table 3, which are taken as the peak loads in this paper. It is not surprising that N_{uc} normally increases with increasing concrete strength, since about 50~70% of the load-carrying capacity is provided by concrete for the tested CFST columns. To quantify the strength improvement of CFST columns with different types of concrete, a strength index (SI) (Wang et al., 2014) is used as shown in Eq. (1):

$$SI = \frac{N_{uc}}{N_0} \quad (1)$$

where $N_0 = f_y A_s + f'_c A_c$; and A_s and A_c are the cross-sectional areas of the steel and concrete, respectively.

The comparison of strength index between the five CFST columns is shown in Fig. 9. The SI -values of the four GCFST columns range from 1.06 to 1.23, and the average value is 1.13. The corresponding value for the reference CFST column is 1.19, which is slightly larger than the average SI -value of the four GCFST columns. If

SI is unity or less, it indicates that the concrete strength enhancement is very weak due to confinement. The higher the value of SI , the higher the concrete confinement. Since SI -values of all the four GCFST columns are larger than unity, it indicates clear confinement of GPC by the steel tube. This is further confirmed by the fact that the steel tube yields well before the peak load, as shown in Figs. 6~8. For the three composite columns with ambient cured GPC, SI -values are 1.13, 1.06 and 1.09 for CFT-GPC1, CFT-GPC2 and CFT-GPC3, respectively. However, specimen CFT-GPC4 with heat cured GPC has the highest SI -value of 1.23. It seems that the heat curing procedure of GPC might have some beneficial influence on the concrete confinement. Further research should be conducted to verify this observation.

3.1.4. Compressive Stiffness

Steel tubes of CFST columns normally exhibit a linear stress-strain relation before yielding. Previous studies have proved that microcracks in concrete lead to a decrease in stiffness as deformation increases (Neville, 2011). The secant stiffness of CFST columns also decreases after cracks develop in concrete core under compression. The compressive stiffness (EA) of a CFST column is defined herein as the secant stiffness corresponding to $0.4N_{uc}$. This definition has also been adopted in a number of previous studies (Yang et al., 2013; Huo et al., 2013; Wang et al., 2017).

According to Wang et al. (2017), the compressive stiffness of circular CFST columns under axial compression can be calculated using Eqs. (2) and (3). The measured compressive stiffness, FE modelling results and predicted results using Wang et al.'s model are compared in Table 4.

$$EA = E_s A_s + \kappa_c E_c A_c \quad (2)$$

$$\kappa_c = \left(\frac{D}{t_s}\right)^{0.004} + \left(\frac{t_s f_y}{D f'_c}\right)^{1.5} \left[56.8 - 56.3 \left(\frac{D}{t_s}\right)^{0.004} \right] \leq 1 \quad (3)$$

where E_c is the Young's modulus of concrete.

It should be noted that the FE modelling is conducted in subsection 3.1.7. When conducting the FE simulation or using Eq. (2), the measured elastic modulus of 194,370 MPa is used for the steel. As E_c was not measured in this test program, Eq. (4) recommended in the Australian standard AS 3600 (2001) was used to predict the elastic modulus for geopolymer concrete with CAC inclusion accord-

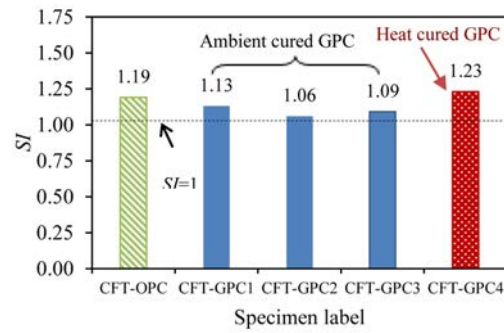


Figure 9. Strength indexes of CFST columns.

ing to an earlier study conducted by the authors (Cao et al., 2018).

$$E_c = 0.043 \times \rho^{1.5} \times \sqrt{f'_c} \quad \text{for } f'_c \leq 40 \text{ MPa} \quad (4a)$$

$$E_c = (0.024 \times \sqrt{f'_c} + 0.12) \times \rho^{1.5} \quad \text{for } f'_c > 40 \text{ MPa} \quad (4b)$$

where ρ is the density of concrete, which was taken as 2368 kg/m³ for GPC based on our previous study (Cao et al., 2018).

The measured values of compressive stiffness EA are plotted in Fig. 10 for comparison. Compared with other specimens, specimen CFT-GPC4 exhibits the least compressive stiffness, due to its lowest strength and the possible liquid phase evaporation during the heat curing process of mix GPC-4. It was also reported in (Hardjito et al., 2004) that heat cured GPC generally has lower elastic modulus than conventional OPC concrete. Furthermore, the concrete strength and compressive stiffness of CFT-GPC1 are also relatively low compared to those of CFT-GPC2 and CFT-GPC3. Meanwhile, it is found that CFT-GPC2 and CFT-GPC3 with ambient cured GPC exhibit higher compressive stiffness than CFT-OPC, although the concrete strengths of the three specimens are very close.

The predicted EA from FE modelling and Eq. (2) are also presented in Fig. 10 for comparison with test data. In general, the EA -values calculated from Eq. (2) are very close to the FE predictions. This is expected since Eq. (2) was developed from numerical data generated from FE modelling. Therefore, only the comparison between the FE predicted and measured EA is discussed as follows. Since the FE model was developed for CFST columns with OPC, it is not surprising that the compressive stiff-

Table 4. Compressive stiffness EA (kN)

Specimen	Measured	FE prediction	Wang et al.'s model
CFT-OPC	809259	854287	841761
CFT-GPC1	717909	762429	760806
CFT-GPC2	984674	852406	882406
CFT-GPC3	917427	875642	892049
CFT-GPC4	624898	718668	717469

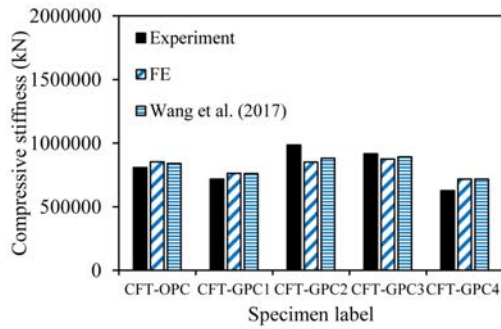


Figure 10. Compressive stiffness of CFST columns.

ness of CFT-OPC has been well predicted by the FE model. For CFT-GPC1, the compressive stiffness is also well predicted with an error of 6.2%. However, the compressive stiffness of CFT-GPC2 is underestimated by 13.4%. In contrast, the compressive stiffness of CFT-GPC4 is overestimated by 14.7%. The divergence between the FE predicted and measured stiffness could be due to two reasons: (1) presence of test error and (2) ignorance of the influence of concrete type in the FE model. Further experimental and numerical studies are required to confirm the reasons.

3.1.5. Ductility

Ductile design of structures is recommended by EN 1998-1 (2004) for seismic-prone zones. Such a design can also mitigate the influence of other extreme events, such as blasts and impact loading. Ductility of a structural component refers to its ability to sustain deformation beyond the elastic limit, whilst maintaining a sufficient load-bearing capacity until failure. The ductility index (DI) (Tao and Han, 2007) expressed by Eq. (5) is used to evaluate the ductility of a CFST column.

$$DI = \frac{\varepsilon_{90\%}}{\varepsilon_y} \quad (5)$$

where $\varepsilon_{90\%}$ is the axial strain when the load decreases to 90% of the ultimate strength; $\varepsilon_y = \varepsilon_{75\%}/0.75$, and $\varepsilon_{75\%}$ is the axial strain when the load attains 75% of the ultimate strength in the pre-peak stage.

Fig. 11 presents the ductility indexes of CFST columns. In general, the columns with lower strength concrete (namely, CFT-GPC1 and CFT-GPC4) exhibit better ductility. The concrete compressive strengths are 37.4 MPa for CFT-GPC1 and 31.8 MPa for CFT-GPC4, respectively. Not surprisingly, the DI -values for the two specimens are very high, which are 30.2 and 18.9, respectively. It is worth noting that CFT-GPC4 has a smaller DI than CFT-GPC1 because the former has a lower compressive stiffness and larger ε_y . The ductility index of the conventional CFST column CFT-OPC ($f'_c = 59.2$ MPa) is 7.1. In contrast, the corresponding GCFST counterparts CFT-GPC2 ($DI = 6.6$, $f'_c = 58.6$ MPa) and CFT-GPC3 ($DI = 4.4$, f'_c

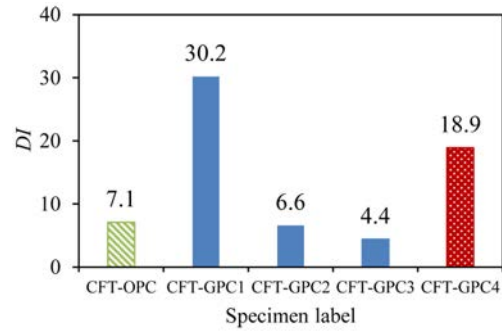


Figure 11. Comparison of different ductility indexes.

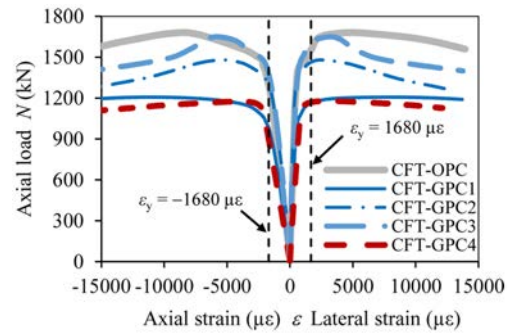


Figure 12. Axial load versus axial and lateral strain curves.

= 64.4 MPa) demonstrate lower ductility, although their concrete strengths are close to that of CFT-OPC. It seems that the use of GPC has some negative influence on the ductility. Dattatreya et al. (2011) and Yost et al. (2013) also observed lower post peak ductility of geopolymer concrete beams compared to conventional OPC concrete beams.

3.1.6. Strain Analysis

The developments of axial (compressive) and lateral (tensile) strains are shown in Fig. 12, where negative strain values indicate compression. The strains are average values of readings from the strain gauges. In general, the steel tubes in all the composite columns develop significant lateral strains because of the Poisson's effect and concrete dilation. Before reaching the ultimate strength, the lateral strains in the steel tubes also exceed the yield strain of steel (ε_y), providing evidence of concrete confinement.

The lateral-to-axial strain ratios (ν) of CFST columns are calculated and the development is illustrated in Fig. 13. The axial load N is normalised with respect to the corresponding peak load N_{ue} for a meaningful comparison. The initial ν -values of all specimens are around 0.3, which is the normal Poisson's ratio for mild steel before yielding (Yu et al., 2016). It can be inferred that no confinement effect on the concrete is provided by the steel tube in this stage. For most CFST columns, the interaction between the steel tube and core concrete becomes apparent with significantly increased lateral-to-axial strain ratio ν , after

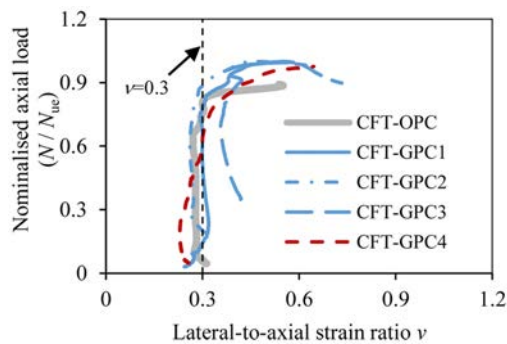


Figure 13. Development of lateral-to-axial strain ratio for CFST columns.

the axial load reaches about 80% of the peak strength. The value of ν soon increases to around 0.5–0.6 at the peak load. It seems that the GCFST columns develop interaction earlier than the reference sample CFT-OPC. However, the lateral-to-axial strain ratio of CFT-OPC increases sharply at the normalised axial load ratio of 0.85. A similar behaviour was reported in a previous study (Yu et al., 2016). In contrast, the lateral-to-axial ratio of the GCFST columns increases more gradually. Another finding is that the lateral-to-axial strain ratio of specimen CFT-GPC4 with heat cured GPC starts to increase at a normalised axial load ratio of around 0.3. This might explain the stronger concrete confinement in this specimen than in other GCFST columns with ambient cured GPC.

3.1.7. Comparison with FE Predictions

For conventional CFST columns, considerable efforts have been made in the past to develop numerical models to predict the mechanical performance. Tao et al. (2013a) collected a wide range of test data to develop a refined FE model for those columns under axial compression. A concrete damaged plasticity material model was implemented to develop a three-stage strain hardening/softening function for concrete confined by the steel tube. The feasibility of using the FE model developed in (Tao et al., 2013a) to predict the performance of GCFST columns at ambient temperature is conducted. It should be noted that research on stress-strain curves of geopolymer concrete is still very limited (Noushini et al., 2016). Under unconfined condition, Hardjito et al. (2005) and Nguyen et al. (2016) reported that the stress-strain model proposed by Collins et al. (1993) for OPC concrete was still applicable to geopolymer concrete. In contrast, Noushini et al. (2016) and Thomas and Peethamparan (2015) reported that geopolymer concrete had a more brittle post-peak response than OPC concrete, which should be reflected in the stress-strain model. Under the confinement of steel spirals, however, the test results presented in (Ganesan et al., 2014) suggest that the stress-strain behaviour of confined geopolymer concrete was very similar to that of confined OPC concrete. Because of a lack of research, the difference

between geopolymer concrete and OPC concrete, if any, is not considered in this study when modelling concrete core confined by the steel tube.

The FE predicted and measured N - ϵ curves of CFT-OPC and other GCFST columns are shown in Fig. 14. For the reference specimen CFT-OPC, the agreement between the predicted and measured N - ϵ curves is reasonable, although the peak load is underpredicted by 8.2%. For the four GCFST columns, satisfactory agreement is also achieved between the predicted and measured N - ϵ curves, although the ultimate strain corresponding to the ultimate strength is slightly overpredicted. The mean and standard deviation of the ratio of measured-to-predicted ultimate capacity are 1.014 and 0.034, respectively, for the four GCFST columns. It should be noted that the ultimate strength of CFT-GPC4 with heat cured GPC is slightly underpredicted by 6.8%. In general, the FE model proposed by Tao et al. (2013a) also gives reasonable predictions of load-deformation curves for GCFST columns.

As pointed out in subsection 3.1.2, the measured ultimate strength is 1681.0 kN for specimen CFT-OPC, which is slightly higher than the corresponding measured value of 1649.9 kN for CFT-GPC3. However, the concrete compressive strength (59.2 MPa) of mix OPC is lower than that (64.4 MPa) of mix GPC-3. As can be seen from Fig. 14, the ultimate strength of CFT-GPC3 is well predicted by the FE model, but the ultimate strength of CFT-OPC is underpredicted by 8.2%. Since the FE model developed by Tao et al. (2013a) has been verified by a wide range of test data of CFST columns with OPC concrete, it can be inferred that the relatively high measured ultimate strength of CFT-OPC is due to test error.

3.2. Performance of CFST Columns after Elevated Temperature Exposure

3.2.1. Failure Modes

The five specimens in Series 2 after testing are shown in Fig. 15. These columns also experienced a local outward folding failure, regardless of the concrete type or strength. The failure mode is similar to the mode of specimens without exposure to elevated temperatures, as presented in Fig. 5.

3.2.2. Axial Load Versus Axial Strain Curves

The axial load versus axial strain (N - ϵ) curves are presented in Fig. 16 for the five specimens tested after exposure to elevated temperatures. As expected, significant deterioration in stiffness and strength is found for all the CFST columns, regardless of the type of concrete. This can be found in Fig. 16a, where a typical column RES-GPC1 is selected to demonstrate the influence of elevated temperature exposure on the N - ϵ curve. In general, the elevated temperature exposure also leads to a significant change in the shape of N - ϵ curves. All unheated specimens either have an obvious post-peak branch or become flat after the ultimate strength. After exposure to elevated temperatures,

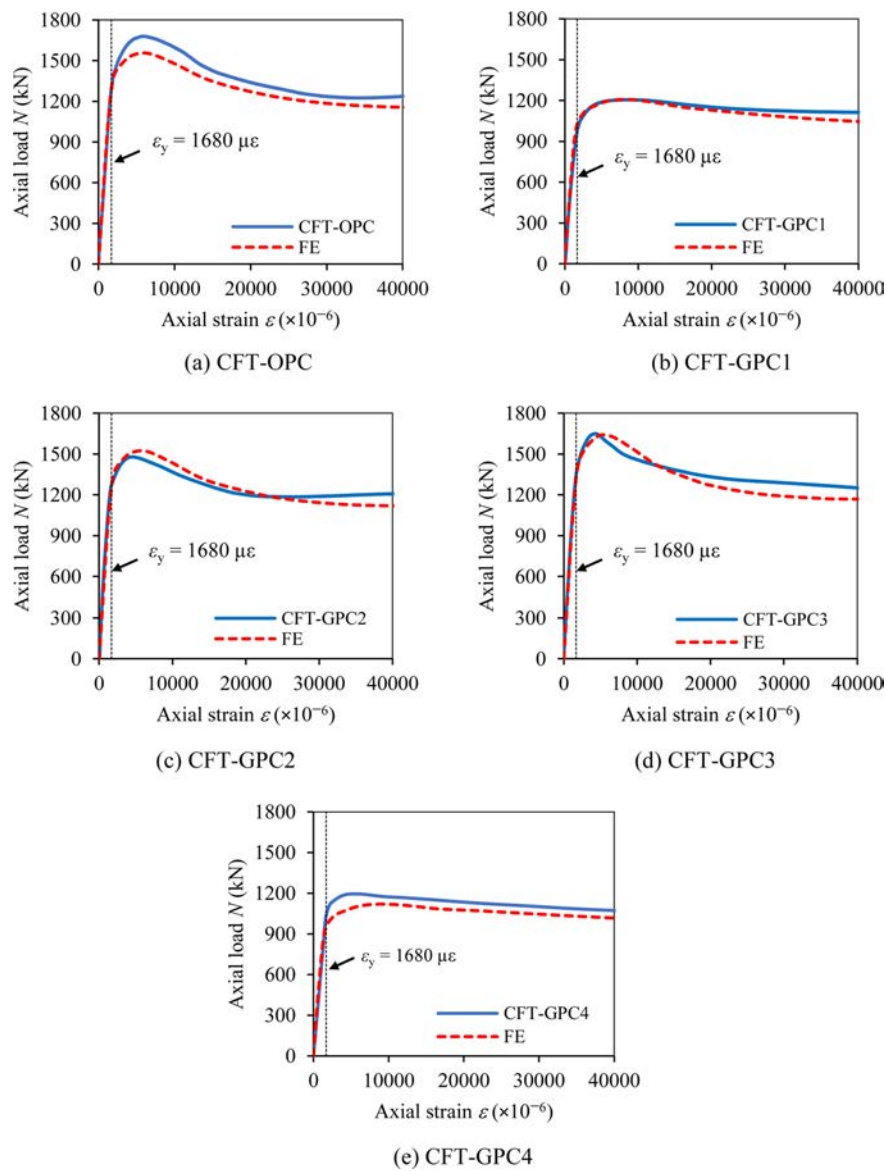


Figure 14. Comparison between measured and predicted N - ϵ curves for composite columns tested at room temperature.



Figure 15. Tested specimens after exposure to elevated temperatures.

the damaged columns show a strain-hardening behaviour, indicating better ductility after the elevated temperature exposure. This is consistent with previous experimental observations on fire-damaged CFST columns (Han et al.,

2002; Li et al., 2017).

Fig. 16b demonstrates the influence of concrete type on the N - ϵ curve for specimens tested after exposure to elevated temperatures. All the specimens have an approxi-

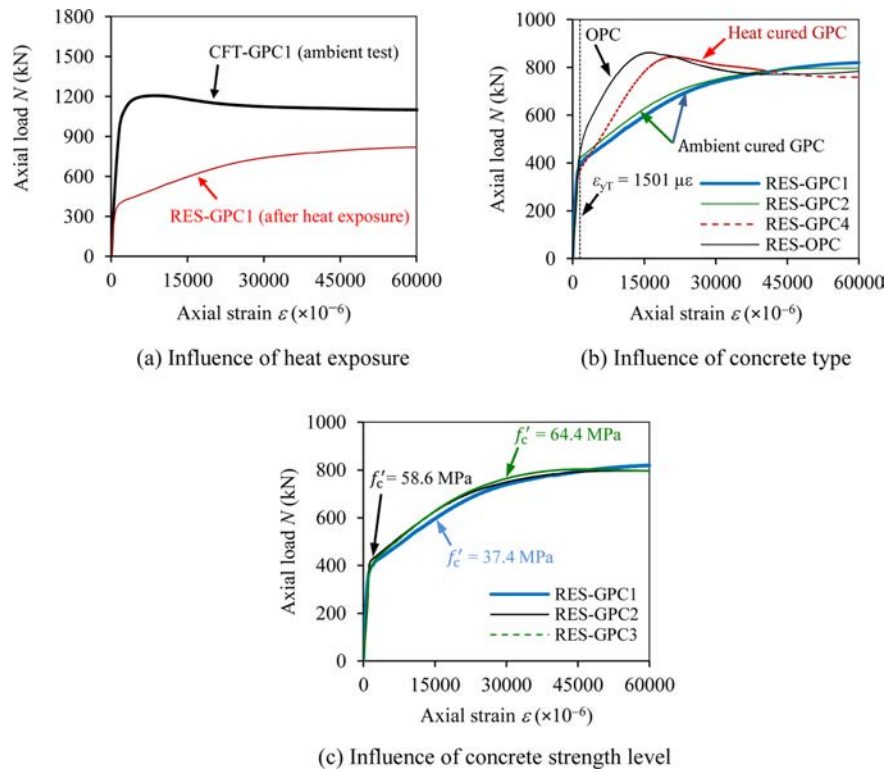


Figure 16. N - ε curves of specimens after elevated temperature exposure.

ately linear response in the initial stage. According to Tao et al. (2013b), the influence of heat exposure on the residual elastic modulus can be ignored for mild steel. Therefore, the yield strain of the steel tube after exposure to 800°C can be calculated as $\varepsilon_{yT} = f_{yT}/E_s$. According to Section 2.4, f_{yT} and E_s can be taken as 291.8 and 194,370 MPa, respectively. Thus, ε_{yT} is determined to be 1501 $\mu\varepsilon$ and indicated in Fig. 16b. As can be seen, the steel yields at an axial load of about 400 kN, followed by a significant decrease in the slope of the curve. This phenomenon is observed in all specimens, but the slope reduction is the least for the reference specimen with OPC, followed by RES-GPC4 with heat cured GPC. The most significant reduction in slope is observed in the GCFST columns with ambient cured GPC. Another interesting finding is that RES-OPC and heat cured RES-GPC4 reach their peak strengths at an axial strain of about 2%, followed by a continuous strength decrease in the post-failure region. However, the load carried by a GCFST column with ambient cured GPC continues to increase until reaching an axial strain of 4%. Beyond this axial strain level, the residual strengths of all the five CFST columns are very close to each other.

The influence of concrete strength on the N - ε curve can be found in Fig. 16c for the three GCFST columns with ambient cured GPC. It seems the influence of concrete strength is very minor on the specimens after heat treatment. All curves roughly overlap each other, indicating

that the different types of concrete have similar residual strength and stiffness. In contrast, the counterpart specimens without elevated temperature exposure have significantly different N - ε curves, as shown in Fig. 16a. Further microstructure analysis is required to investigate ambient cured GPC after exposure to elevated temperatures.

3.2.3. Residual Strength

Specimens RES-OPC and RES-GPC4 have a post-peak branch and their peak strengths (N_{max}) are 862.7 and 844.4 kN at axial deformations of 1.63% and 2.11%, respectively. In contrast, RES-GPC2 and RES-GPC3 have peak strengths of 796.6 and 804.7 kN corresponding to much larger axial deformations of 5.84% and 4.60%, respectively. Furthermore, the strength of RES-GPC1 kept increasing until the test finished at the axial deformation of 6%; the corresponding strength of 820.4 kN is taken as N_{max} for this specimen. Compared with the reference specimen RES-OPC, all GCFST columns have slightly lower values of N_{max} . However, the difference is not significant and the reduction in N_{max} ranges from 2.1% to 7.7%.

Since the peak strength of a damaged CFST column is reached at a relatively large deformation, this strength is unlikely to be fully utilised in the post-fire assessment and reinstatement. Following the definition proposed by Tao et al. (2013a), the residual ultimate strength ($N_{u,r}$) is defined as the load at the axial strain of 0.01. The value of $N_{u,r}$ is presented in Table 3 for each specimen. Compared

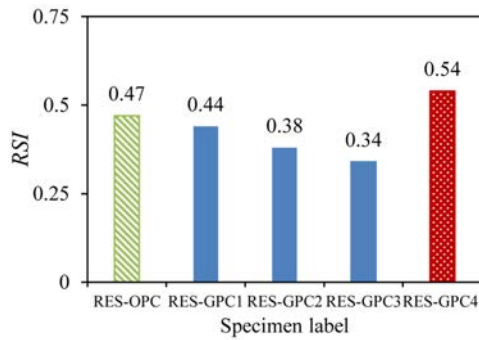


Figure 17. Comparison of different residual strength indexes.

with N_{max} , a reduction of 8.7% is found for $N_{u,r}$ of the reference specimen RES-OPC. However, the reduction ranges from 23.8% to 35.6% for GCFST columns due to their much smaller slopes in the second region of the $N-\varepsilon$ curves.

A residual strength index (RSI) (Tao and Han, 2007) defined in Eq. (6) is used to quantify the strength loss of CFST columns after heat treatment.

$$RSI = \frac{N_{u,r}}{N_{ue}} \quad (6)$$

where N_{ue} is the ultimate strength of the counterpart specimen without exposure to elevated temperature.

A comparison between different CFST columns on the residual strength index is shown in Fig. 17. Obviously, the strength losses are different for CFST columns with different types of concrete core. The heat cured GCFST column (RES-GPC4) with a RSI -value of 0.54 exhibits superior heat resistance than other columns, whereas the corresponding ratio is 0.47 for the reference specimen RES-OPC. However, other GCFST columns with ambient cured GPC have a higher strength loss than RES-OPC; their RSI values range from 0.34 to 0.44. The RSI value decreases as the compressive strength of GPC cured at ambient temperature increases, although the residual strength recovers to some extent at a large deformation for the three GCFST columns with ambient cured GPC. Further research is required to improve the residual strength of ambient cured GPC by optimising the mix design.

3.2.4. Residual Compressive Stiffness

The definition of residual compressive stiffness (EA) which is the secant stiffness corresponding to the residual strength of $0.4N_{u,r}$ is similar to the definition of compressive stiffness for specimens tested at ambient temperature. The test results are compared in Fig. 18. After the heat treatment, RES-GPC3 and RES-GPC4 have similar compressive stiffness as the reference sample RES-OPC, whereas RES-GPC2 has lower compressive stiffness than the reference sample. For RES-GPC1 with a relatively low concrete strength, its compressive stiffness is larger than

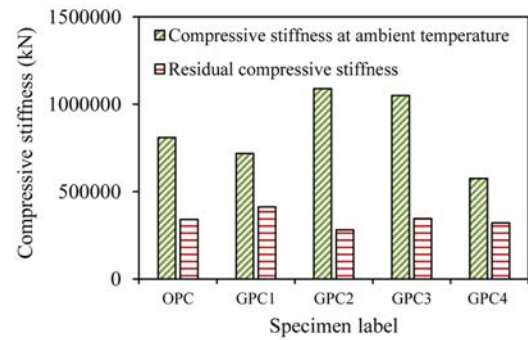


Figure 18. Compressive stiffness of CFST columns after exposure to elevated temperatures.

that of the reference sample. It seems a GCFST column with a higher concrete strength has a higher loss in compressive stiffness.

3.3. Performance of CFST Columns under Combined Temperature and Loading

The specimens in Series 3 are presented in Fig. 19 after tested under combined temperature and load. Since these specimens were tested in a load-control model, they failed abruptly with substantial deformation developed at the end of testing. In general, the failure occurred near the top endplate and stiffeners; they assisted the heat transfer because they were close to the heating elements.

Fig. 20 shows the comparison of axial deformation versus time ($\Delta-t$) relationships for different specimens. Typically, the $\Delta-t$ curve of a CFST column has three stages (Tao et al., 2016) where in the initial stage, the column starts to expand because of the thermal expansion. Then the column starts to contract gradually due to strength loss at an elevated temperature. Finally, as the elevated temperature duration increases, the axial contraction deformation of the column increases sharply. The column fails when the remaining load-bearing capacity is no longer able to support the applied load. The current specimens have an initial load ratio of 0.5, which is relatively large. Therefore, only specimen HOT-GPC2 experienced initial thermal expansion lasting for about 35 min; other specimens started to contract once the furnace temperature increased. The obvious initial thermal expansion for HOT-GPC2 is likely due to the addition of extra water in the mix GPC-2. The evaporation of water during the heat exposure could absorb a large amount of heat, which delayed the heat transfer from the outside to the inside. Consequently, the growth rate of load-induced axial shortening would be affected. Although extra water was also added in GPC-4, it might have evaporated during the heat curing.

The fire resistance (t_R) of CFST columns under combined temperature and loading are presented in Table 3. The conventional CFST column (HOT-OPC) exhibits the



Figure 19. Failed specimens under combined temperature and loading.

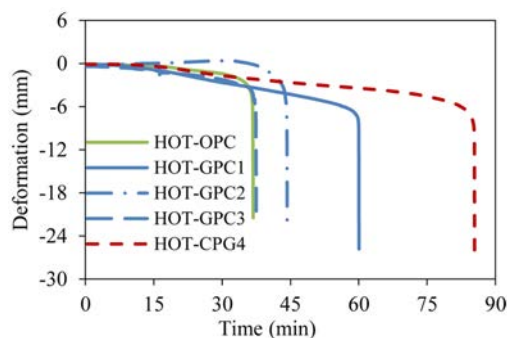


Figure 20. Axial deformation versus time curves of CFST columns subjected to elevated temperatures.

worst fire endurance, which achieved a t_R of 36.7 min. By comparison, the heat cured GCFST column HOT-GPC4 has the best fire endurance, maintaining its integrity under elevated temperatures for 85.4 min. Similar to the residual strength tests on GCFST columns, ambient cured GCFST columns with low concrete strength level exhibit better fire endurance. For example, HOT-GPC1 obtained a fire resistance of 60.1 min. The fire endurance of HOT-GPC3, which has high strength GPC ($f'_c = 64.4$ MPa), is worse like HOT-OPC. Clearly, further research is required to improve the fire performance of ambient-cured high strength GPC.

4. Conclusions

This paper has presented the experimental results and numerical modelling results of concrete-filled steel tubular (CFST) columns tested at room temperature, and also reported the results of CFST columns tested at elevated temperatures and exposure to elevated temperatures. Geopolymer concrete (GPC) was used to fill the majority of the steel tubes. Reference specimens made from ordinary Portland cement (OPC) concrete were also prepared and tested. The following conclusions can be drawn within the scope of this study:

(1) The mechanical properties (i.e., the initial stiffness, ultimate strength and concrete confinement effect) of geopolymer concrete-filled steel tubular (GCFST) columns at ambient temperature are similar to those of conventio-

nal CFST columns.

(2) The existing FE model proposed by Tao et al. (2013a) can also be used to predict the load-deformation curves of GCFST columns at ambient temperature, and the prediction accuracy is reasonably good.

(3) GCFST columns exhibit better fire resistance than the conventional CFST column, especially when heat cured GPC is used. After exposure to elevated temperatures, GCFST columns with ambient cured GPC have larger strength loss than the reference conventional CFST column. In contrast, the GCFST column with heat cured GPC exhibits superior heat resistance than other columns.

Acknowledgements

The authors are grateful for the financial support from Australian Research Council Linkage Grant No. LP16010 1484. The authors would like to acknowledge the technical support from the laboratory staff Mr Murray Bolden and Mr Robert Marshall.

References

- ASTM C39, Standard Test Method for Compressive Strength of Cylindrical Concrete Specimens, ASTM International, West Conshohocken, PA, USA, 2001.
- AS 3600-2001. Australian Standard, Concrete structures. Sydney, Australia, 2001.
- Ataei, A., Bradford, M.A., Liu, X. (2016). "Experimental study of composite beams having a precast geopolymer concrete slab and deconstructable bolted shear connectors." *Eng. Struct.*, 114, 1-13.
- Cao, Y., Tao, Z., Pan, Z., Murphy, T.D., Wuhler, R. (2016). "Effect of calcium aluminate cement on workability and compressive strength of fly ash geopolymer mortar cured at ambient temperature." *Proceedings of the 24th Australasian Conference on the Mechanics of Structures and Materials*, Perth, Australia, 927-932.
- Cao, Y.F., Tao, Z., Pan, Z., Wuhler, R. (2018). "Effect of calcium aluminate cement on geopolymer concrete cured at ambient temperature." *Constr. Build. Mat.* 191, 242-252.
- Collins, M.P., Mitchell, D., MacGregor, J.G. (1993). "Structural design considerations for high-strength concrete." *ACI Concr. Int.*, 15 (5), 27-34.
- Dattatreya, J.K., Rajamane, N.P., Sabitha, D., Ambily, P.S., Nataraja, M.C. (2011). "Flexural behaviour of reinforced geopolymer concrete beams." *Int. J. Civ. Struct. Eng.*, 2 (1), 138-159.
- EN 1998-1. Design of Structures for Earthquake Resistance – Part 1: General Rules, Seismic Actions and Rules for Buildings, European Committee for Standardization (CEN), Brussels, Belgium, 2004.
- Espinosa, A., Romero, M.L., Hospitaler, A., Pascual, A.M., Albero, V. (2015). "Advanced materials for concrete-filled tubular columns and connections." *Struct.*, 4, 105-113.
- Ganesan, N., Abraham, R., Raj, S.D., Sasi, D. (2014). "Stress-strain behaviour of confined geopolymer conc-

- rete." *Constr. Build. Mater.*, 73, 326-331.
- Habert, G., Lacaille, J.D.E. De, Roussel, N. (2011). "An environmental evaluation of geopolymer based concrete production: reviewing current research trends." *J. Clean. Prod.*, 19(11), 1229-1238.
- Han, L.H., Li, W., Bjorhovde, R. (2014). "Developments and advanced applications of concrete-filled steel tubular (CFST) structures: Members." *J. Constr. Steel Res.*, 100, 211-228.
- Han, L.H., Yang, H., Cheng, S.L. (2002). "Residual strength of concrete filled RHS stub columns after exposure to high temperatures." *Adv. Struct. Eng.*, 5(2), 123-134.
- Hardjito, D., Wallah, S., Sumajouw, D., Rangan, B. (2004). "The stress-strain behaviour of fly ash-based geopolymer concrete." *Developments in Mechanics of Structures and Materials*, A A Balkema Publishers, The Netherlands, 831-834.
- Hardjito, D., Wallah, S., Sumajouw, D., Rangan, B. (2005). "Introducing fly ash-based geopolymer concrete: Manufacture and engineering properties." *Proceedings of the 30th Conference on Our World in Concrete and Structures*, 271-278.
- Huo, J., Zhang, J., Wang, Z., Xiao, Y. (2013). "Effects of sustained axial load and cooling phase on post-fire behaviour of reinforced concrete stub columns." *Fire Saf. J.*, 59, 76-87.
- ISO 834, Fire-resistance Tests — Elements of Building Construction — Part 1: General Requirements, International Standard ISO 834, Geneva, Switzerland, 1999.
- Kodur, V., Phan, L. 2007. "Critical factors governing the fire performance of high strength concrete systems." *Fire Saf. J.*, 42(6-7), 482-488.
- Li, X., Bao, Y., Xue, N., Chen, G. (2017). "Bond strength of steel bars embedded in high-performance fiber-reinforced cementitious composite before and after exposure to elevated temperatures." *Fire Saf. J.*, 92, 98-106.
- Li, W., Luo, Z., Tao, Z., Duan, W.H., Shah, S.P. (2017). "Mechanical behavior of recycled aggregate concrete-filled steel tube stub columns after exposure to elevated temperatures." *Constr. Build. Mat.*, 146, 571-581.
- Mo, K.H., Alengaram, U.J., Jumaat, M.Z. (2016). "Structural performance of reinforced geopolymer concrete members: A review." *Constr. Build. Mat.*, 120, 251-264.
- Neville A.M. *Properties of Concrete* (Fifth Edition), Pearson Education Limited, Harlow, England, 2011.
- Nguyen, K.T., Ahn, N., Le, T.A., Lee, K. (2016). "Theoretical and experimental study on mechanical properties and flexural strength of fly ash-geopolymer concrete." *Constr. Build. Mater.*, 106, 65-77.
- Noushini, A., Aslani, F., Castel, A., Gilbert, R.I., Uy, B., Foster, S. (2016). "Compressive stress-strain model for low-calcium fly ash-based geopolymer and heat-cured Portland cement concrete." *Cem. Concr. Compos.*, 73, 136-146.
- Ozbakkaloglu, T., Xie, T. (2016). "Geopolymer concrete-filled FRP tubes: Behavior of circular and square columns under axial compression." *Comp. Part B: Eng.*, 96, 215-230.
- Pan, Z., Sanjayan, J.G. (2012). "Factors influencing softening temperature and hot-strength of geopolymers." *Cem. Con. Comp.*, 34(2), 261-264.
- Pan, Z., Tao, Z., Cao, Y., Wuhler, R., Murphy, T. (2018). "Compressive strength and microstructure of alkali-activated fly ash/slag binders at high temperature." *Cem. Con. Comp.*, 86, 9-18.
- Shaikh, F., Vimonsatit, V. (2015). "Compressive strength of fly-ash-based geopolymer concrete at elevated temperatures." *Fire Mat.*, 39(2), 174-188.
- Shi, X.S., Wang, Q.Y., Zhao, X.L., Collins, F.G. (2015). "Structural behaviour of geopolymeric recycled concrete filled steel tubular columns under axial loading." *Constr. Build. Mat.*, 81, 187-197.
- Sumajouw, M., Rangan, B.V. *Low-calcium fly ash-based geopolymer concrete: Reinforced beams and columns*, Research Report GC 3, Faculty of Engineering, Curtin University of Technology, Perth, Australia, 2006.
- Sumajouw, D., Hardjito, D., Wallah, S., Rangan, B. (2007). "Fly ash-based geopolymer concrete: Study of slender reinforced columns." *J. Mat. Sci.*, 42(9), 3124-3130.
- Tao, Z., Ghannam, M., Song, T.Y., Han, L.H. (2016). "Experimental and numerical investigation of concrete-filled stainless steel columns exposed to fire." *J. Constr. Steel Res.*, 118, 120-134.
- Tao, Z., Ghannam, M. (2013). "Heat transfer in concrete-filled carbon and stainless steel tubes exposed to fire." *Fire Saf. J.*, 61, 1-11.
- Tao, Z., Wang, Z.B., Yu, Q. (2013). "Finite element modelling of concrete-filled steel stub columns under axial compression." *J. Constr. Steel Res.*, 89, 121-131.
- Tao, Z., Wang, X.Q., Uy, B. (2013). "Stress-strain curves of structural and reinforcing steels after exposure to elevated temperatures." *J. Mater. Civ. Eng.*, 25(9), 1306-1316.
- Tao, Z., Han, L.H. (2007). "Behaviour of fire-exposed concrete-filled steel tubular beam columns repaired with CFRP wraps." *Thin-Walled Struct.*, 45(1), 63-76.
- Thomas, R.J., Peethamparan, S. (2015). "Alkali-activated concrete: Engineering properties and stress-strain behavior." *Constr. Build. Mat.*, 93, 49-56.
- Vickers, L., Pan, Z., Tao, Z., Van Riessen, A. (2016). "In situ elevated temperature testing of fly ash based geopolymer composites." *Fire Mat.*, 9(6), 445-458.
- Wang, Y., Burgess, I., Wald, F., Gillie, M. *Performance-based fire engineering of structures*, CRC Press, Taylor & Francis Group, 2012.
- Wang, W.H., Han, L.H., Li, W., Jia, Y.H. (2014). "Behavior of concrete-filled steel tubular stub columns and beams using dune sand as part of fine aggregate." *Constr. Build. Mat.*, 51, 352-363.
- Wang, Z.B., Tao, Z., Han, L.H., Uy, B., Lam, D., Kang, W.H. (2017). "Strength, stiffness and ductility of concrete-filled steel columns under axial compression." *Eng. Struct.*, 135, 209-221.
- Yang, H., Han, L.H., Wang, Y.C. (2008). "Effects of heating and loading histories on post-fire cooling behaviour of concrete-filled steel tubular columns." *J. Constr. Steel Res.*, 64(5), 556-570.
- Yang, Y.F., Cao, K., Wang, T.Z. (2013). "Experimental behavior of CFST stub columns after being exposed to freezing and thawing." *Cold Regions Sci. Tech.*, 89, 7-21.

- Yost, J.R., Radlinska, A., Ernst, S., Salera, M., Martignetti, N.J. (2013). "Structural behavior of alkali activated fly ash concrete. Part 2: structural testing and experimental findings." *Mater. Struct.*, 46, 449-462.
- Yu, X., Tao, Z., Song, T.Y. (2016). "Effect of different types of aggregates on the performance of concrete-filled steel tubular stub columns." *Mater. Struct.*, 49(9), 3591-3605.